Hindawi
Advances in Materials Science and Engineering
Volume 2022, Article ID 4310662, 14 pages
https://doi.org/10.1155/2022/4310662

Research Article

Investigation on the Effect of Butyl Acrylate (nBA) to Improve the Toughness Properties of Methacrylate-Based Waterproofing Adhesive Material (MMA) for the Steel Bridge Deck

Mengya Zhang

College of Management, Xi'an University of Finance and Economics, Xi'an 710100, China

Correspondence should be addressed to Mengya Zhang; zhangmy@xaufe.edu.cn

Received 16 February 2022; Accepted 23 April 2022; Published 27 May 2022

Academic Editor: Pietro Russo

Waterproof adhesion materials (WAL) for steel bridge decks should have comprehensive strong bonding capabilities to steel substrates/pavement layers, water resistance, and persistence to harsh conditions. Methacrylate-based adhesive (MMA), as a typical WAL material for steel bridge decks, lacks sufficient flexibility and diverse compatibility. In this article, flexible, stabile at high temperature, and well-bonded poly (methyl methacrylate)/n-butyl acrylate copolymer [poly(MMA-r-nBA)] coatings were developed with toughening as a breakthrough point. The above properties are obtained by forming an interpenetrating network through interchain van der Waals forces. In addition to the flexibility provided by the long-chain structure of n-butyl acrylate, its unique molecular structure allows it to improve the high-temperature stability and lower the glass transition temperature of MMA. Due to the reduced glass transition temperature, it can also be matched to various pavement layers. Thus, the poly(MMA-r-nBA) composite polymer coatings can be applied to steel bridge decks that require long-term service in various conditions.

1. Introduction

In the application of steel bridge deck engineering, waterproof adhesion layers (WAL) are commonly required to firmly adhere to both steel substrates and pavement layers [1]. Also, they need to be water-resistant and be persistent to harsh conditions (such as cyclic loading and extreme temperature) [2–5] and economical. Although various WAL materials have been developed to achieve engineering applications under different conditions, it remains a major challenge to fulfill all the requirements [6, 7]. For example, epoxy adhesives provide good mechanical properties, chemical resistance, and corrosion resistance. However, they are more sensitive to temperature, and adhesive failure can easily occur at high temperatures [8]. Solvent-based rubber asphalt is convenient for construction and has high impermeability, but its gas release can easily lead to the blistering of the pavement layer under the action of high-temperature paving [9]. Methacrylate-based adhesive (MMA) has been widely used for steel bridge decks because of its good properties, including good water resistance, resistance to high and low temperature, and high mechanical strength [10]. Compared to epoxy adhesives, MMA can provide better bonding strength at high temperatures, which will benefit steel bridge deck applications in high-temperature zones. Compared with asphalt-based adhesives, MMA has better water resistance, chemical resistance, and bonding properties. However, in accordance with coating applications, MMA material lacks sufficient flexibility and diverse compatibility for steel bridge decks. In our previous work, the bonding capacity of MMA material on various pavement layers was investigated and found to be poorly compatible with epoxy asphalt concrete (EA). It is prone to adhesive failure even at room temperatures [11]. Also, the MMA and upper asphalt mixture separated rapidly and completely after shear damage. This phenomenon was due to the high molecular chain rigidity and poor flexibility of the MMA after adhesive failure. An improved solution in terms of the molecular structure of the waterproofing adhesive material is highly desired to address these issues and challenges.

Recently, by taking the advantages of free radical polymerization [12, 13] in regulating physical properties through chemical crosslinking [14–16], people have developed various coating materials with unique features of high-temperature resistant, fast-curing, flexibility, elasticity, and toughness [17]. Current research pointed out that adding soft monomers to the hard monomers can be a solution for improving its toughness and durability [18, 19]. n-butyl acrylate (nBA), as a typical soft monomer, has good weathering resistance, chemical resistance, and flexibility for multifunctionality [20, 21]. Polymerization contributes to the modification of the physical and chemical properties of MMA. In this study, combining the advantages of both, poly (methyl methacrylate)/n-butyl acrylate copolymer [poly(-MMA-r-nBA)] is proposed as a new WAL material for the steel bridge deck. The bonding capacity of poly(MMA-r-nBA) and their derivatives as WAL for steel bridge decks have been rarely reported. The effect of the chemical groups providing flexibility on the performance of the waterproofing bonding layer is still unknown. This project predicted the optimal molecular ratio and poly(MMA-r- nBA) properties through molecular dynamics simulations. It used several microscopic experimental methods to explore the copolymer toughening mechanism. Finally, the poly(MMA-r-nBA) properties were verified by using indoor pull-out/shear tests.

2. Materials and Methods

2.1. Materials. Methacrylate-based adhesive (MMA), which includes two-component methyl methacrylate resin (A/B), and benzoyl peroxide (BPO) were procured from Chi Road, Chongqing Technology Co., Ltd. Pavement, China. n-Butyl acrylate (nBA), 2,2′-Azobis(2-methylpropionitrile) (AIBN), sodium dodecyl sulfate (SDS), N,N-dimethyl p-toluidine (DMT), and ethanol were purchased from Nanjing Chemical Reagent Co., Ltd. This article selected two typical steel bridge deck protective layers: guss asphalt concrete (GA-10) and epoxy asphalt concrete (EA-10), respectively. The optimal asphalt content (by mass of aggregate) of GA-10 is 7.5% and EA-10 is 6.3%.

2.2. Methods

2.2.1. Sample Preparation. Poly(MMA-r-nBA) was prepared via emulsion polymerization technology, starting with MMA and nBA mixed in required proportions before transferring to the flask-3-neck. Here, the ratio of nBA was set to be 70:40. The reaction mixture comprises monomers (60 g total), AIBN (0.24 g) as the initiator, surfactant SDS (0.3 g), and ethanol (30 g) as the bulk medium for emulsion. The experiment with the starved semi-continuous addition of the initiator to the reaction mixture was used. The reaction was conducted using a magnetic stirrer (5 hrs, 400 rpm) at 75°C. Finally, 0.1 wt% N, N-dimethyl p-toluidine (DMT) (promoter) and 2 wt% BPO (initiator) were added to the solution to achieve a shorter curing time. As a control group, the MMA system was prepared via the first manual mixing of 2 wt% benzoyl peroxide (BPO) and the "B" component. The "A" component was then added to the mixture equivalent to the 1 : 1 A/B ratio. The experimental plan is shown in Figure 1.

2.2.2. Molecular Dynamic Simulations. Materials Studio 8.0 was employed to construct MMA and nBA homopolymers and poly (MMA-r-nBA) random copolymer. The polymethyl methacrylate (pMMA)polymer structures were available in the repeat unit list of system libraries, while the polybutyl acrylate (pnBA) polymer structure was obtained from Urban's work [22] and then generated with the sketching tools provided in Materials Visualizer. The copolymer (methyl methacrylate/n-butyl acrylate) can be randomized according to the specified molar ratios of the units. All simulated polymers consisted of 7 chains with a length of 20 units each. The poly (MMA-r-nBA) molar ratios were varied from 30/70 to 70/30. The settings are shown in Table 1.

The initial density of each MMA/nBA composition cell was 0.5 g/cm^3. All cells were built at room temperatures and one atmospheric pressure (standard pressure). Before equilibration, the systems were subjected to geometrically optimized using 5,000 iterations. The copolymer structure was relaxed for 10 cycles to eliminate irrational energy by annealing from 600 K to 200 K. Upon completion, a 200 psec isothermal–isasteric (NVT) ensemble with a time step of 0.5 fs was used to obtain primary values of minimized energies. The unit cell was further equilibrated by using a 600-psec isothermal–isobaric (NPT) ensemble with a time step of 1 fs to reach the real density. The Nosé-Hoover (NHL) thermostat and Berderson barostat were used to control, respectively, the temperature and pressure of the system during the simulation. The changes in potential energy, temperature, and density of the system with time were monitored during dynamics. The system could be stable when these values remain constant or slight fluctuation around the constant value. The COMPASS force field was utilized in all MD simulations.

2.2.3. Analytical Methods. The thermal property and thermal decomposition temperature of poly(MMA-r-nBA) were measured using a NETZSCH TGA/DTG analyzer (TG 209 F3). The synthetic milky fluid was cast onto a petri dish and let evaporate for 24 h at room temperatures. Then, the formed film was dried at 40°C for 1 day in a vacuum oven to remove the last traces of solvent and then quenched to room temperature. Film samples ranging from 6 to 10 mg were placed in an alumina ceramic crucible and heated under an N2 atmosphere (flow rate: 100 mL/min) from 30 to 600°C with a heating rate of 10°C/min.

Data for the dynamic mechanical properties, such as storage modulus (E′), loss modulus (E″), and loss factor Tanδ[log(E″)/log(E′)] were determined using Dynamic mechanical analysis (DMA), which was performed using a TA Instrument Q800 DMA under dual cantilever bending mode. Each specimen was cut to 35 mm (length) × 10 mm (width) × 5 mm (height). All experiments were repeated

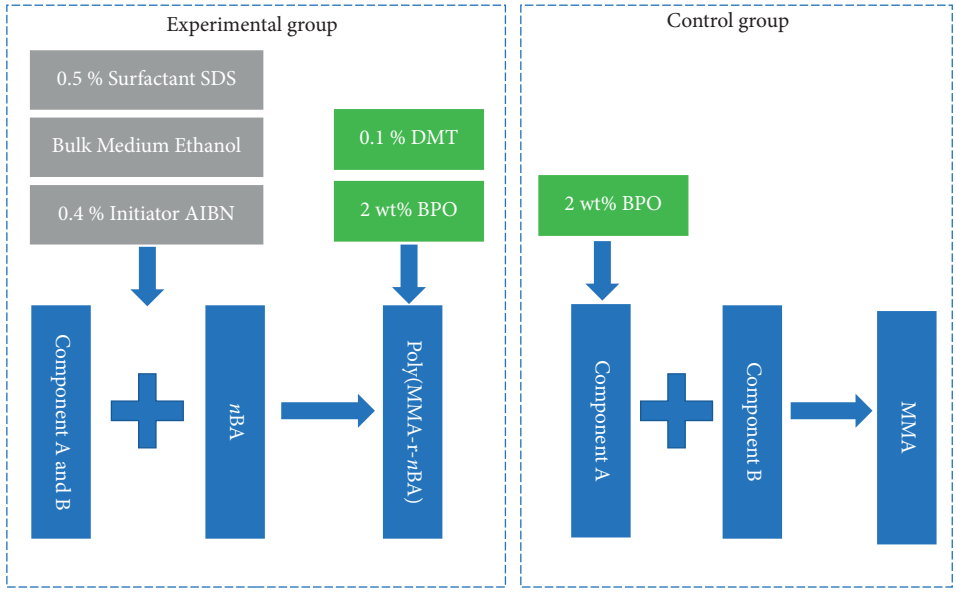

Figure 1: Experimental plan for sample preparation.

Table 1: The parameters of poly(MMA-r-nBA) atomistic models.

MMA/nBA compositions	Degree of polymerization	Number of chains	Initial density (kg/m^3)	Number of atoms	Box size (Å3)
100/0	20	7	0.5	2114	36.0 × 36.0 × 36.0
70/30	20	7	0.5	2366	37.0 × 37.0 × 37.0
55/45	20	7	0.5	2618	37.9 × 37.9 × 37.9
50/50	20	7	0.5	2555	37.7 × 37.7 × 37.7
45/55	20	7	0.5	2681	38.1 × 38.1 × 38.1
40/60	20	7	0.5	2744	38.3 × 38.3 × 38.3
30/70	20	7	0.5	2933	39.0 × 39.0 × 39.0
0/100	20	7	0.5	3374	40.4 × 40.4 × 40.4

twice. The analysis was performed from −30 to 100°C with 5°C/min heating rate at 1 Hz frequency.

Transform Infrared Spectroscopy in ATR mode (FTIR-ATR) was used to identify the structure of the poly (MMA-r-nBA). The infrared spectra of the dried poly (MMA-r-nBA) copolymer were taken with a spectrophotometer (Bruker Vertex 70) in the wavenumber range of 400–4000 cm^{-1} with a resolution of 2 cm^{-1}.

The surface morphology stretched/unstretched poly (MMA-r-nBA) films were taken using a Zeiss Sigma 300 scanning electron microscopy (SEM). All samples were examined using operating conditions with voltage 0.1–30 kV, probe current 20 nA, counting time 60 s, and secondary electron images were acquired. The surfaces of the sectioned specimens were gold-coated to eliminate electrostatic charging when using SEM to test. The stretched/unstretched samples used dumbbell-shaped test pieces of the cured poly(MMA-r-nBA) and MMA. The samples' geometry was in accordance with ASTM D638, as illustrated in Figure 2. The tensile tests were performed for stretched samples using a universal material testing machine (ZWICK Z020). The samples were cured at room temperatures for 96 h before demolding and 25°C for 72 h after demolding. The tensile test was then performed at a 2 mm/min crosshead rate, with the initial separation between the chucks being 25 mm. Unstretched samples were damaged after being kept in liquid nitrogen for a certain time (usually 15 min) as a control group. Fresh sections of all the samples are taken for observation and analysis.

Figure 2: Geometry of tensile sample.

The pull-off test was used to investigate the adhesive property of poly(MMA-r-nBA)-Steel plate interface, as shown in Figure 3. The specimen consisted of a steel plate (with corrosion protection layer) descaled by sand to Sa2.5 grade and four 17-mm diameter pullers. The metal pullers were bonded to the steel plate by poly (MMA-r-nBA)

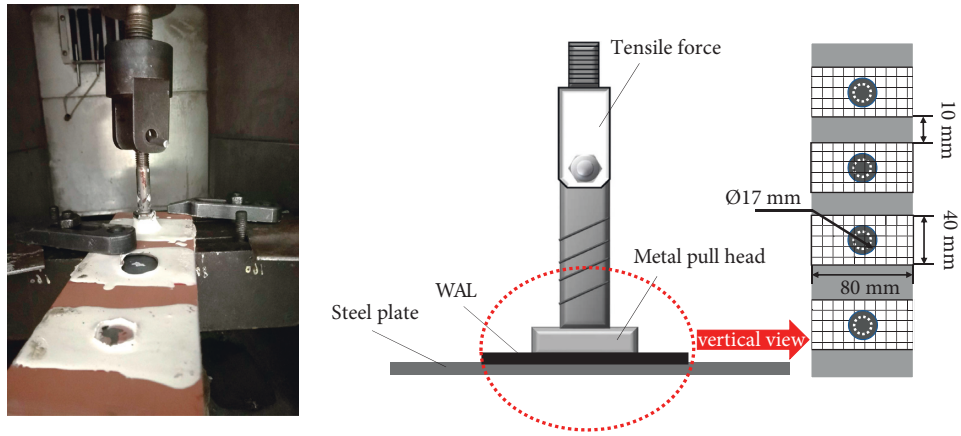

Figure 3: Steel plate-poly(MMA-r-nBA) pull-off test.

copolymer. A gap of 10 mm between adjacent pullers was maintained to ensure that the load path was not disturbed. The tensile speed is set at 10 mm/min. Pull-off tests were performed at different test temperatures (80°C, 60°C, 25°C, 5°C). Three parallel specimens need to be used for each measurement. All the samples were maintained at the test temperature before testing. "MMA-Steel plate" was used as the comparison group with the same specimen method. The following formula calculated tensile strengths:

$$\sigma = \frac{F}{S}, \tag{1}$$

where σ is pull-off strength, MPa; F is maximum tension, kN; S is bonding area, mm.

The pull-off and direct shear tests were performed using MTS universal material testing machine. The experiments were tested under 10 mm/min displacement control at 25°C and 60°C to investigate the poly(MMA-r-nBA) and the pavement layer (GA/EA) bonding properties. An "asphalt mixture + steel plate + asphalt mixture" structure [300 mm (width) × 300 mm (length) × 100 mm (height)] was cut, which resulted in a tested sample of size 80 mm × 50 mm × 80 mm (see Figure 4(a)). The pull-off and shear test can be performed separately by changing the orientation of the fixture (see Figures 4(b) and 4(c)). Notably, the steel plate [300 mm (width) × 300 mm (length) × 3 mm (height)] was sandblasted and then sprayed with an anti-corrosion layer on both sides. Three parallel groups were conducted fo each experiment. The samples were maintained at the test temperature before testing. The strengths were calculated as follows:

$$\tau = \frac{F}{S}, \tag{2}$$

where τ is shear strength, MPa; F is maximum tension, kN; S is shear area, mm.

3. Results and Analysis

3.1. Influence of Molecular Ratios on poly (MMA-R-nBA) Properties. Molecular simulation work can be used to predict the macroscopic properties of materials, optimize the materialization and synthesis process, and provide feasible experimental solutions. In this way, the aim is to reduce the blindness of research and save cost and time. Therefore, molecular dynamics (MD) simulations were used as a function of copolymer composition to determine the optimal molar ratio of the copolymers. Van der Waals Force (vdWeq), density (ρ), and free volume (FV) are shown in Figure 5 (Table 2). The composite copolymer can be divided into three stages from the range of vdW force and copolymer density variation. The equilibrium Van der Waals Force (vdWeq) (curve a), as well as the density (ρ) (curve b), both reach the maxima for 40/60 and 50/50 MMA-r-nBA compositions (rangeII). The copolymerization of MMA-r-nBA depended on the vdW force and the state of molecular chain aggregation. The chemical reaction between nBA and MMA increased the side chains on the MMA molecules. The free volume (FV) acts as a tunnel to transport the penetrant molecules, which can be used to determine the gap between the molecules. As shown in Table 2, the free volume for most of the copolymer was lower than that of homopolymer, especially for 40/60 MMA-r-nBA compositions. However, 70/30 and 30/70 MMA-r-nBA compositions showed an opposite trend because the copolymer interchain aggregation was more significant within range II. In contrast, ranges I and III exhibited fewer interdigitation chains (Figure 5). Within range II, the extended-chain helix-like conformations resulted in increasing energy of the system, which was reflected by the maximum vdWeq density (2.135×105 kJ/m^3). Therefore, it can be concluded that copolymers with 45/55–50/50 MMA-r-nBA molar ratios have better molecular chain interactions. For the comparative study of p (MMA-r-nBA) polymer properties, three schemes with molar ratios of 40/60, 70/30, and 50/50 were used in the subsequent experiments.

3.2. Thermodynamic Properties of poly(MMA-R-nBA) Copolymer. The thermal property and thermal decomposition temperature of poly(MMA-r-nBA) were characterized using a NETZSCH TGA/DTG analyzer (Figures 6(a) and 6(b) for TG stage curves and DTG curves of the samples, respectively). The addition of nBA significantly affected the

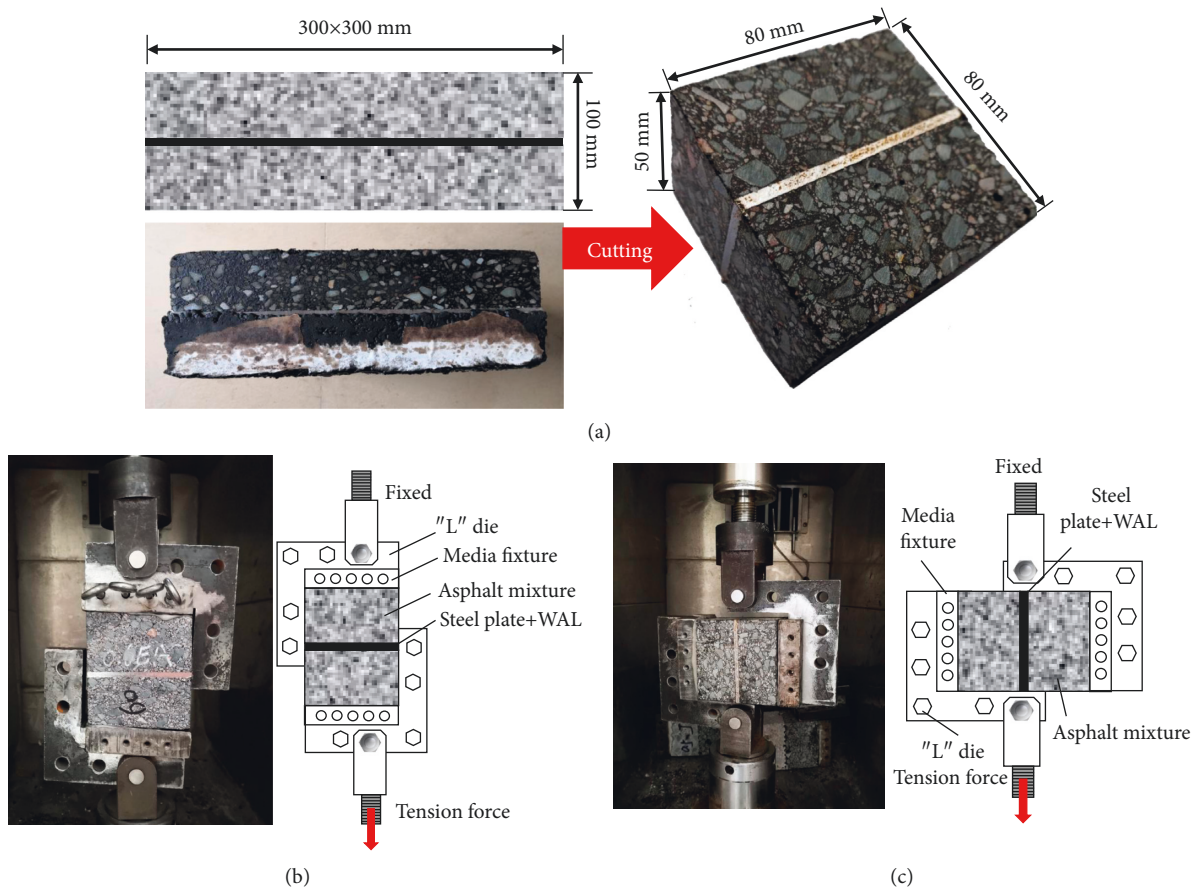

Figure 4: Testing sample and testing machine. (a) Preparation process, (b) pull-off test, and (c) direct-shear test.

thermal stability of the poly(MMA-r-nBA) copolymer. Significant differences can be found when comparing the decomposition stages and temperature of the pure MMA and poly (MMA-r-nBA) copolymers at each stage (Table 3). It can be seen that MMA has achieved more than 10% mass loss at 302.1°C. While the poly (MMA-r-nBA) copolymers with different molar ratios increased the second stage decomposition temperature of MMA by 19.5°C, 31.8°C, and 16.9°C, respectively. The degradation temperatures information can be obtained by the TG derivative curves of the four samples at a maximum rate of weight-loss [23]. It can be seen from the DTG curves that the whole thermal decomposition process of the samples can be divided into four stages. Also, the thermal decomposition behavior of poly(MMA-r-nBA) and MMA were consistent. The first weight-loss stage occurs at about 240°C for all the samples. The loss was due to the vaporization of the remaining water in the polymers. There was a slight loss of water from the material during the heating process, proving that the waterproofing composite materials had excellent water resistance. The DTA curves of the samples in the second weight-loss stage (240–350°C) shown in Figure 6(b) suggest that the peak positions of poly(MMA-r-nBA) were higher than that of MMA. This phenomenon can be explained as the addition of nBA can effectively inhibit the decomposition of MMA molecular chains under high temperatures [24]. The introduction of pnBA improved the thermal properties of MMA by releasing reactive free radicals at higher temperatures. These radicals combine with the chains generated by MMA in the initial stages of depolymerization to form more stable materials, thereby inhibiting further degradation of MMA. However, the poly(MMA-r-nBA) peak position gradually decreased beyond 370°C, indicating that the inhibitory effect began to fail. The thermal stability of the composites showed a significant improvement as the nBA increases, which was beneficial to the full play of the waterproofing materials under a high paving temperature. Significantly, 50/50 poly(MMA-r-nBA) residual weight was maximum at 410°C, about 37.4%. Therefore, a 50/50 poly(MMA-r-nBA) provides higher thermal stability and more adequate soft and hard segment interactions.

Assuming the chain entanglements are the primary contributors to decreased glass-transition temperature [log(E″)/log(E′))] and enhanced flexibility experimentally obtained in dynamic mechanical analysis (DMA), the storage modulus (E′) of MMA and 50/50 poly(MMA-r-nBA) showed a maximum value of 453 MPa and 22 MPa at −20°C, respectively. It may be due to the higher relative density at low temperatures, as shown in Figure 6(c). The E' values for MMA and 50/50 poly(MMA-r-nBA) were nearly identical when the temperature exceeds 70°C. The accelerated mobility of polymer chains increased the

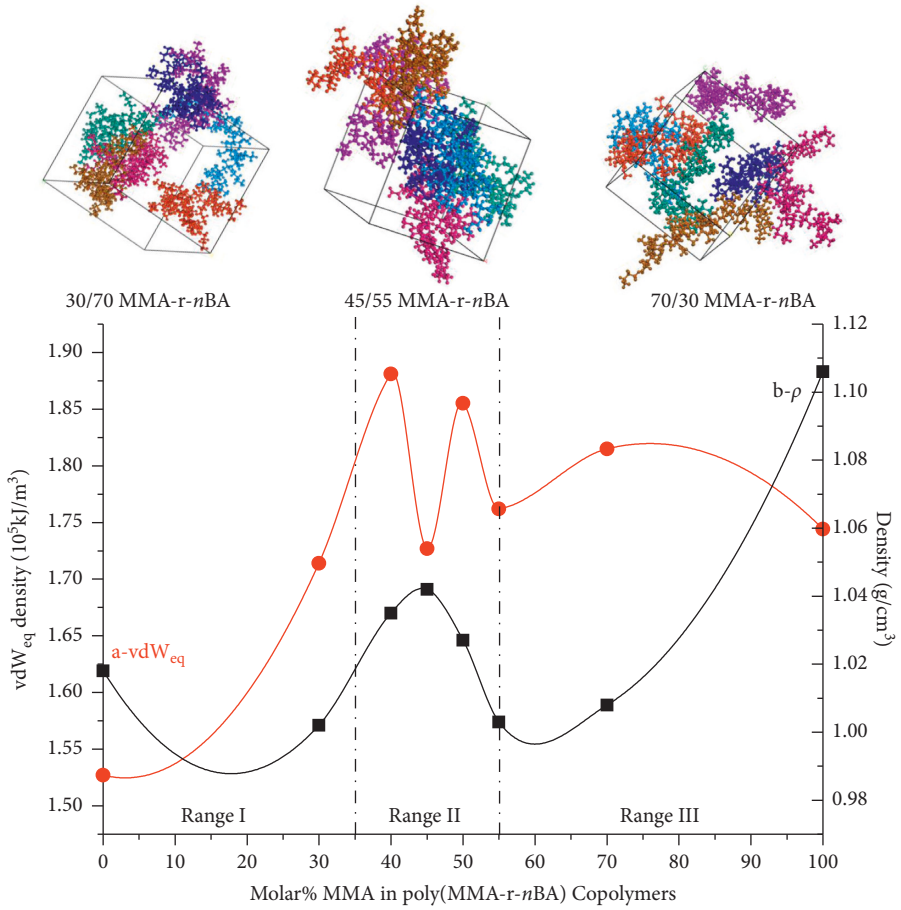

Figure 5: MD simulation results as a function of poly(MMA-r-nBA) copolymer composition. Trend of van der Waals Force (vdWeq) (curve (a) as well as the density (ρ) (curve (b) as a function of poly(MMA-r-nBA) copolymers with different molar ratios.

Table 2: Cohesive energy density of equilibrated (CEDeq), van der Waals (vdW) density, free volume (FV), density (ρ), and solubility parameter (δ) as a function of MMA-r-nBA molar ratios.

MMA-r-nBA molar ratio	Density (kg/m^3)	CEDeq (105 kJ/m^3)	vdW density (105 kJ/m^3)	Δ (J/m^3)1/2	FV (Å)
100/0	1.106	2.029	1.744	14.103	5907.46
70/30	1.008	2.093	1.815	14.466	6436.50
55/45	1.003	1.992	1.762	14.113	5265.87
50/50	1.027	2.112	1.855	14.532	5118.32
45/55	1.042	1.98	1.727	14.006	5100.43
40/60	1.035	2.135	1.881	14.612	4306.58
30/70	1.002	1.923	1.714	13.862	6233.73
0/100	1.018	1.712	1.527	12.941	5561.97

dissipation energy under high temperatures, which decreased the deformation resistance property of materials. However, the E′ value of 50/50 poly(MMA-r-nBA) was smaller than that of MMA material, mainly due to the energy dissipation phenomenon caused by the coordinated movement of polymer chains. The sharp decrease in the modulus of the MMA material correlated very well with incorporating the soft monomer nBA and the network structures in the two polymers. Further evidence for interchain interactions can be found in determining the glass-transition temperature. The tanδ curve of both MMA and 50/50 poly(MMA-r-nBA) showed a single peak, indicating only one glass transition temperature, 85.16°C and 30.01°C, respectively (Figure 6(d)). The lower glass-transition temperature and modulus were due to the molecular structural changes. Thus, DMA results can reasonably assume the expected formation of random and/or alternating chain topologies in poly(MMA-r-nBA) copolymer coatings. However, this remains insufficient to clarify the toughening mechanism of nBA.

3.3. Structural Characterization of poly(MMA-R-nBA) Copolymer. Any small changes in molecular composition or structure can change the material properties [25, 26]. The

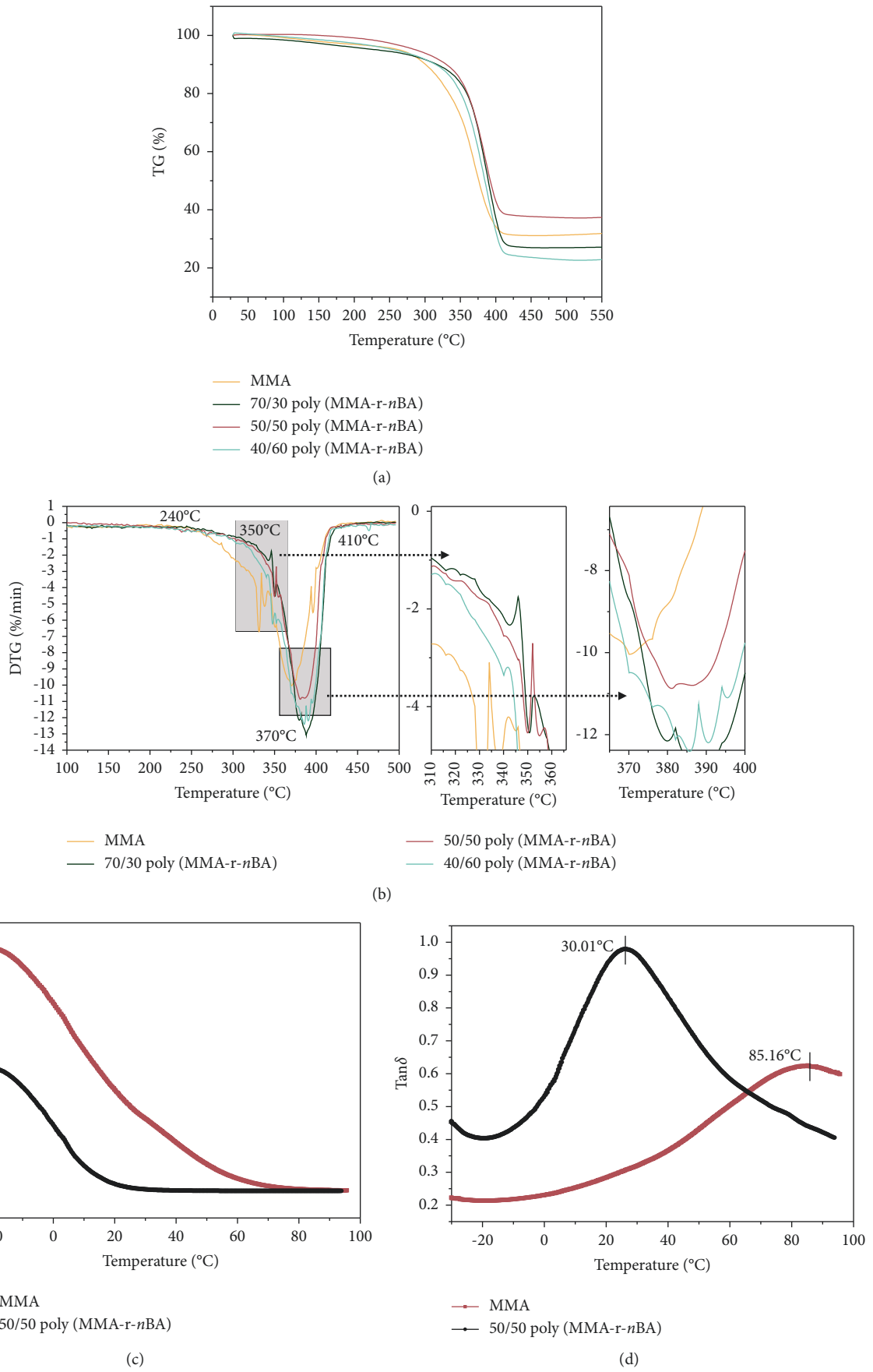

Figure 6: Continued.

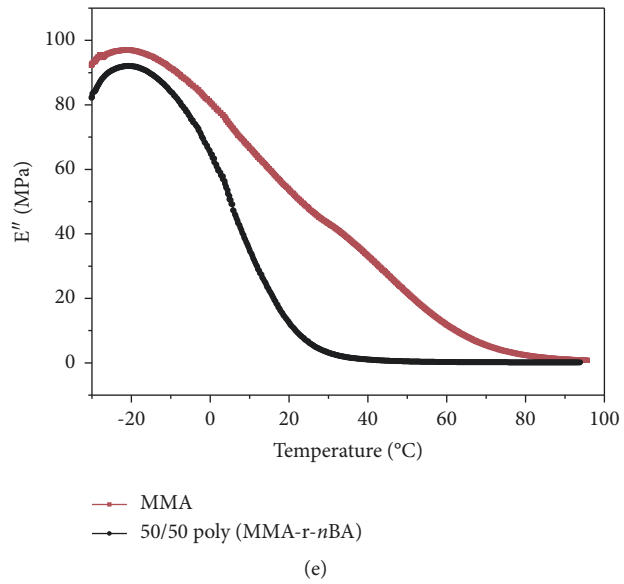

Figure 6: Thermal property of polymers and their mechanical analysis. (a) TG stage curves of the MMA and poly(MMA-r-nBA) polymers. (b) DTG curves of the MMA and poly(MMA-r-nBA) polymers; The two grey boxes represent peaks at approximately 350°C and 370°C, respectively. (c-e) DMA curves of the MMA and 50/50 poly(MMA-r-nBA) samples. The test data includes storage modulus, loss factor (Tg), and loss modulus.

Table 3: Polymer decomposition results with temperature.

Sample	First decomposition		Second decomposition		Third decomposition		Final decomposition	
	T5 (°C)	Weight loss (wt%)	T10 (°C)	Weight loss (wt%)	T50 (°C)	Weight loss (wt%)	Tf (°C)	Weight loss (wt%)
MMA	264.1	5.00	302.1	10.26	376.1	50.05	398.0	65.78
70/30 poly(MMA-r-nba)	237.6	5.09	321.6	10.13	393.0	50.75	428.0	72.59
50/50 poly(MMA-r-nba)	289.9	5.07	333.9	10.35	393.9	49.72	428.0	61.90
40/60 poly(MMA-r-nba)	261.0	5.06	319.0	10.16	387.0	49.35	428.0	75.72

Note : T5, T10, T50 is the temperature of 5%, 10%, 50% of weight loss, respectively ; Tf is the final stage temperature.

crosslinking efficiently introduced a long side-chain connecting the MMA main chains, which was beneficial for improving the toughness of the coatings (Figure 7(a)–7(d). Fourier Transform infrared spectroscopy (FTIR) was performed to evaluate how the introduction of nBA changes the molecular structure of MMA. The polymer chemical bonding changes and elemental relative concentration information were evaluated. Taking 50/50 poly(MMA-r-nBA) as a typical example, the addition of nBA to MMA revealed a partial shift of the band, a decrease in the intensity of some bands, and a disappearance of some bands. As shown in Figure 7(b), MMA monomers exhibited strong peaks at 2850 cm^{-1}, assigned to -CH3 rocking vibration in methacrylate. The peak from 1780 to 1670 cm^{-1} of 50/50 poly(MMA-r-nBA) indicated that C=O stretching vibration at 1728 cm^{-1} from the ester group in MMA is preserved in 50/50 poly(MMA-r-nBA). The peak at 810 cm^{-1} was abolished after forming 50/50 poly(MMA-r-nBA) through crosslinking via emulsion polymerization. These spectral bands changed with increasing or decreasing methyl methacrylate composition in the polymer. Methylene functional groups (-CH2) replaced the original methyl side chains (-CH3), suggesting that the nBA was attached to the MMA structure, consistent with the theoretical reaction structure.

3.4. Microscopic Morphology of poly(MMA-R-nBA) Copolymer. The high-temperature stability of the poly(-MMA-r-nBA) can be attributed to the increased number of flexible side chains and the unique network interpenetration structure of poly(MMA-r-nBA), both of which contributed to increasing the copolymer toughness. In general, the increased flexibility of the coating made the energy required to delaminate the interface from the substrate per unit area increase, expressed as a cohesive failure. Adding soft monomers affected the mechanical properties of MMA by comparing the surface and cross-sectional morphology of

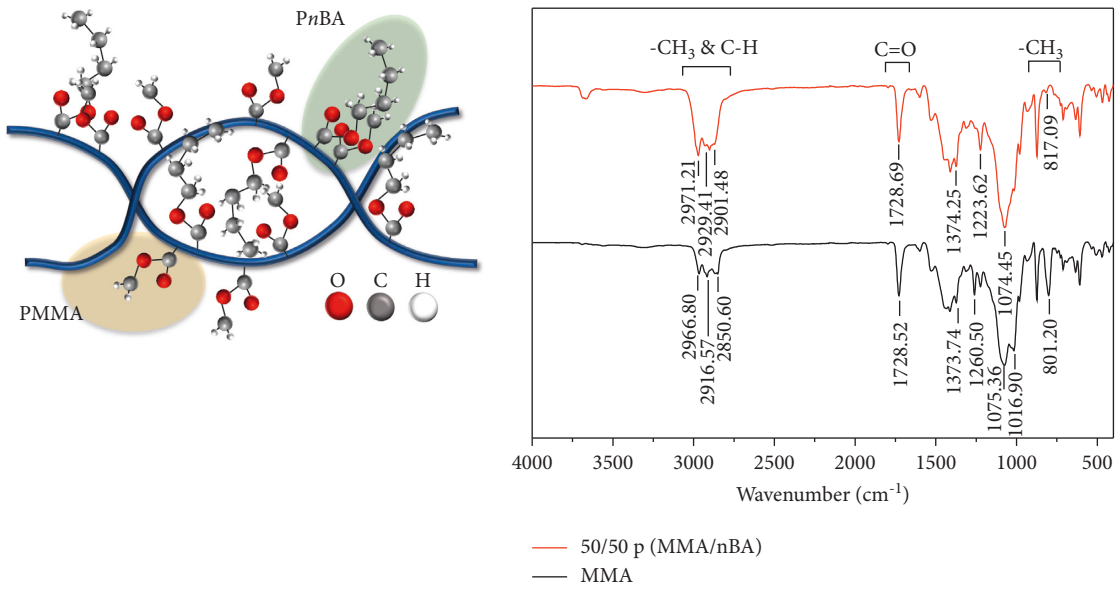

Figure 7: Molecular configuration of poly(MMA-r-nBA) coatings and proposed toughness mechanism. (a) Chemical structure of the poly(MMA-r-nBA) copolymer; the hard monomer (pMMA) and soft monomer (pnBA) units are indicated by yellow and green color, respectively. (b) ATR-FTIR spectra shows the comparison intensities of chemical groups in the MMA(black) and 50/50 poly(MMA-r-nBA) (red), respectively.

polymers before and after stretching with different molar ratios. Figure 8(b) shows the microstructure of the stretched/unstretched surfaces for poly(MMA-r-nBA) copolymers with 40/60 to 70/30 poly(MMA-r-nBA) molar. The unstretched poly(MMA-r-nBA) surface was relatively flat, indicating that the poly(MMA-r-nBA) molecular chain was randomly aligned before the stretch. On the contrary, a small amount of tensile texture appeared on the surface of 70/30 poly(MMA-r-nBA) after stretching. Then 50/50 poly(MMA-r-nBA) displayed a large number of continuous, oriented textures. Moreover, 40/60 poly(MMA-r-nBA) also has obvious stretching textures, but interruptions exist. It was shown that the 70/30 poly(MMA-r-nBA) has less tensile deformation due to maximum stiffness. In comparison, 50/50 and 40/60 poly(MMA-r-nBA) have obvious tensile deformation and behave as ductile fractures. However, the stress distribution in the molecular chain was increasingly inhomogeneous when the tensile strength of the material itself was exceeded. The macromolecular chains will easily pull off or slip due to the lower stiffness of 40/60 poly(MMA-r-nBA), forming more fracture sources. Figure 8(c) illustrated the microstructure of the stretched/unstretched cross-sections for poly(MMA-r-nBA) copolymers with 40/60 to 70/30 poly(MMA-r-nBA) molar. The fracture of the unstretched specimen was flat, while the drawing fracture has a character of dimple fracture. In general, the size and depth of the dimple are related to the ductility of the material [27]. With the increase of nBA content, the number of dimples increased gradually, and the morphology changed from shallow to deep, the edge changed from sharp to smooth, indicating the transformation of poly(MMA-r-nBA) composites from brittle fracture to ductile fracture. The variation in polymer surface/section morphology at different molar ratios confirmed that the increase in nBA monomer reduced the material stiffness and increased the tensile fracture rate.

3.5. Pull-Off and Direct Shear Results. As a waterproof adhesive material, the adhesion/shear strength of poly(MMA-r-nBA) on various substrates (steel and asphalt mixture) was subsequently evaluated. The optimal spaying amount of poly(MMA-r-nBA) was selected as 1.5 kg/m^2 according to the "Specifications for Design and Construction of Pavement on Highway Steel Deck Bridge" (China, JTG/T3364-02-2019). The poly(MMA-r-nBA) was compared with MMA material under the same spraying amount to verify its performance. The adhesive strength of MMA to steel plate was about twice that of poly(MMA-r-nBA), indicating that the toughness of nBA to MMA was obtained by sacrificing a certain adhesive strength. However, the interface between the waterproof layer and asphalt mixture was the weak point in the structure of the "asphalt mixture + steel plate + asphalt mixture" [28]. The bond strength of poly(MMA-r-nBA) with asphalt mixture should be deeply investigated.

The delamination between the steel plate and paving layer usually does not occur at low temperatures. Thus, this article was investigated at 25°C and 60°C. From Figures 9(b) and 9(c), the compatibility of MMA with GA was better than that of poly(MMA-r-nBA) at room temperatures. The shear strength of the "MMA + GA" structure was about twice that of the " poly(MMA-r-nBA) +GA" structure, 0.7 MPa and 0.35 MPa, respectively. However, the maximum interfacial adhesion strength of the former and the

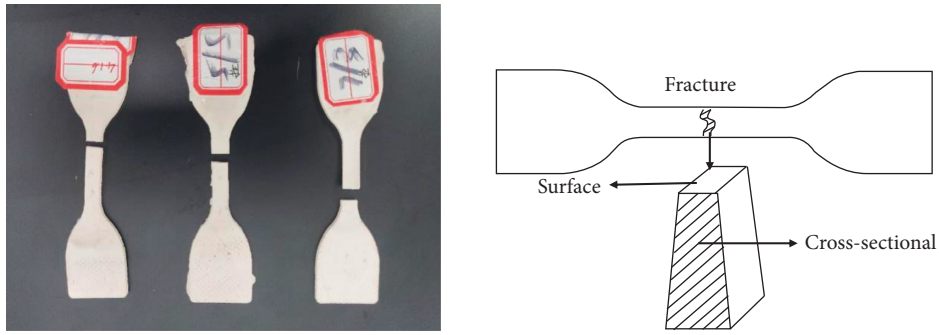

(a)

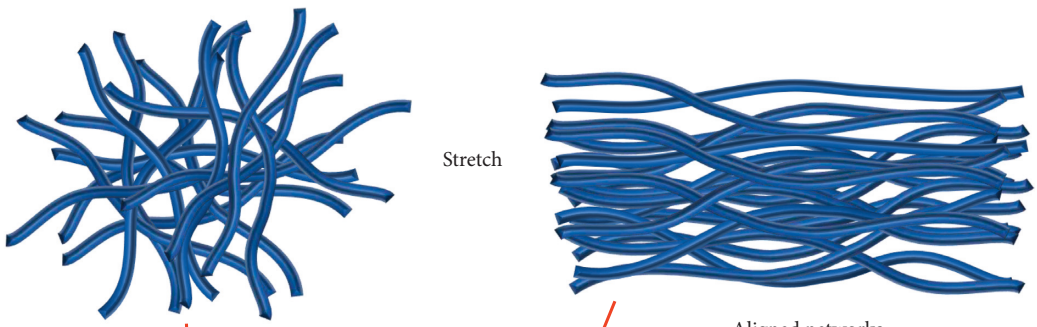

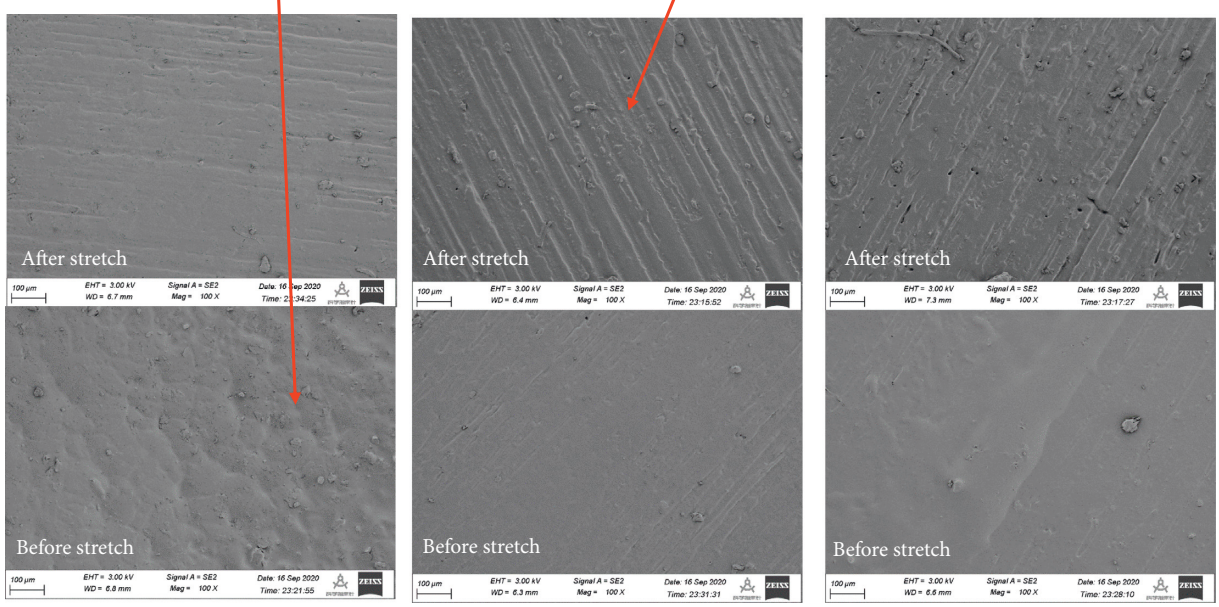

70/30 poly (MMA-r-*n*BA) | 50/50 poly (MMA-r-*n*BA) | 40/60 poly (MMA-r-*n*BA)

(b)

Figure 8: Continued.

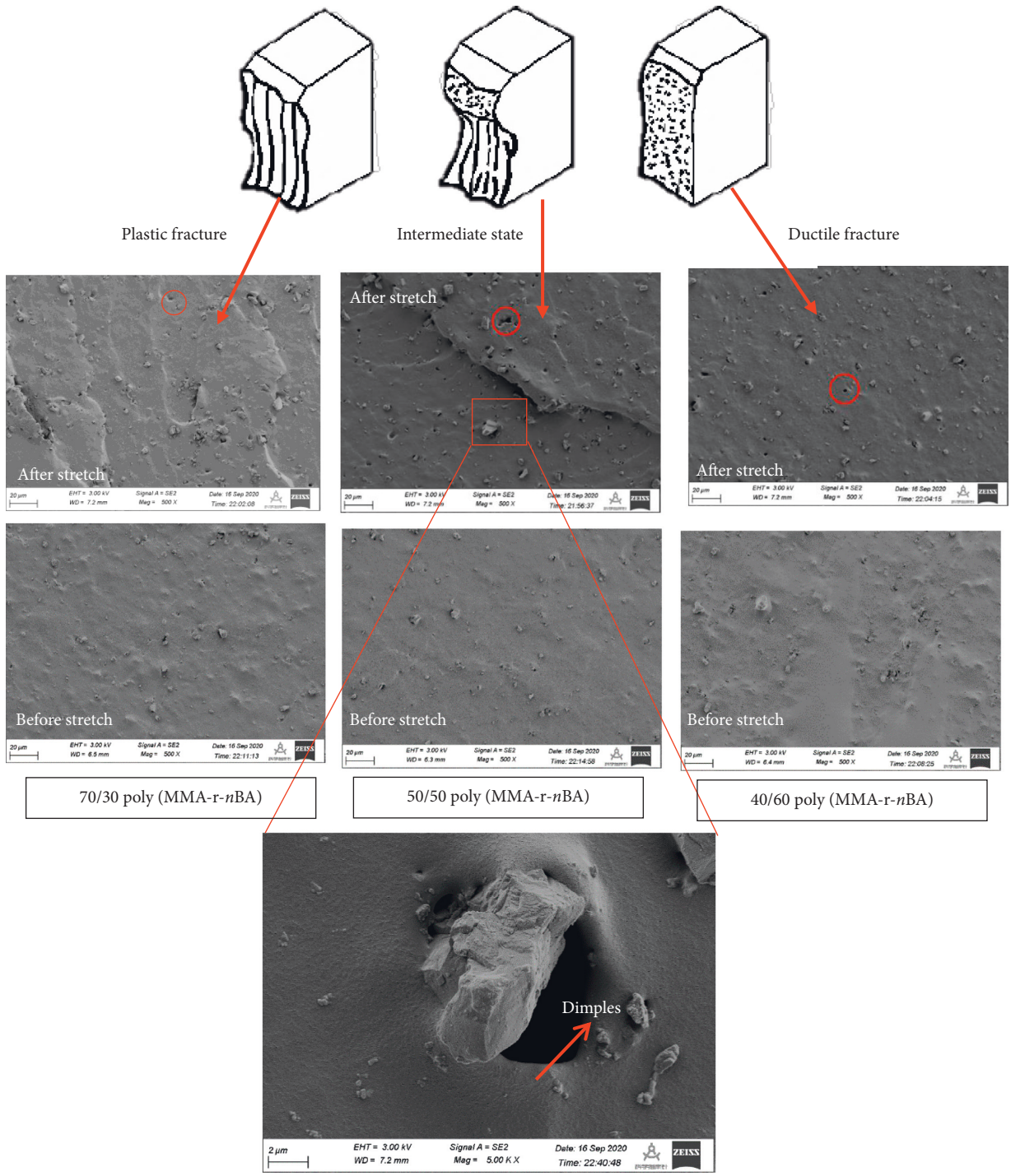

(c)

Figure 8: (a) SEM test samples and the diagram of the test area. (b) A comparison of the micromorphology between the poly(MMA-r-nBA) with different molar ratios before and after the samples are stretched. Here, samples are chosen from the fracture surface. (c) Cross-sectional SEM image of the poly(MMA-r-nBA) with different molar ratios before and after the samples are stretched; and a magnified view of the dimple region is shown.

latter were basically the same. The adhesion strength of MMA was significantly reduced to 0.02 MPa when the protective layer was EA, which was only 12% of the "poly(MMA-r-nBA)+EA" structure (0.16 MPa). Moreover, the shear strength of the "MMA + EA" structure (0.03 MPa) was only 7% of the "poly (MMA-r-nBA) +EA" structure (0.38 MPa). The results showed that the compatibility of MMA and EA was dramatically weaker than poly(MMA-r-nBA). The interlayer damage can easily occur even at room temperatures.

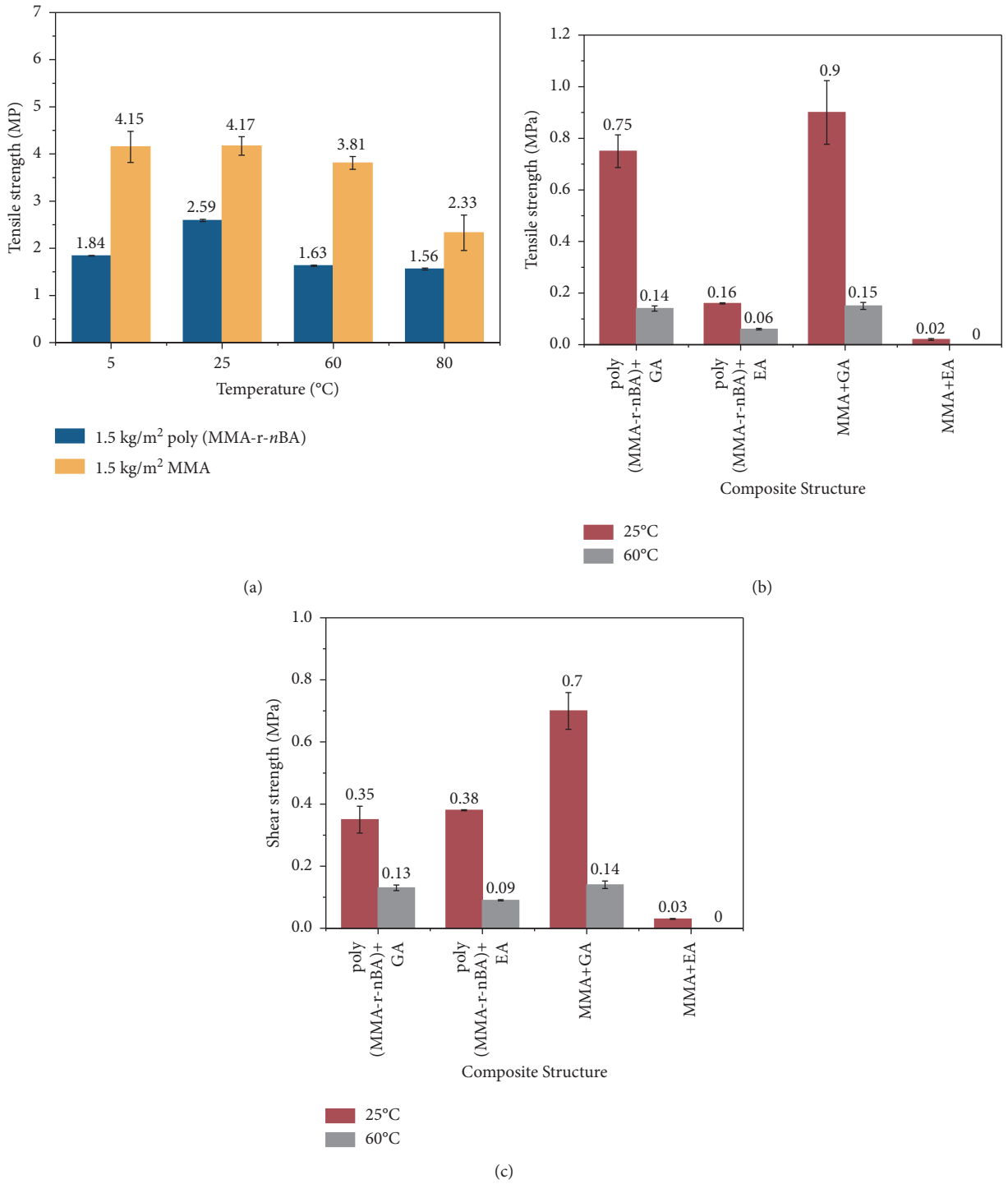

Figure 9: Comparison of adhesive and shear strengths between MMA and the poly(MMA-r-nBA) coatings. (a) The adhesive strength between the poly(MMA-r-nBA) coating and steel substrates (yellow columns) and, as a comparison, the results of MMA adhesive materials (blue columns) are listed. (b) The adhesive strength between the poly(MMA-r-nBA)/MMA coating and asphalt mixture (GA and EA). (c) The shear strength between the poly(MMA-r-nBA)/MMA coating and asphalt mixture (GA and EA). Further details are given in Table 4.

The difference in tensile/shear strength between the "MMA + GA" and "poly(MMA-r-nBA)+GA" structures was not significant at 60°C. When the protective layer was EA, the tensile/shear strength of the "MMA + EA" structure was almost 0 MPa, while the tensile and shear strength of the "poly (MMA-r-nBA)+EA" specimen were 0.06 MPa and 0.09 MPa, respectively. The poor compatibility between MMA and EA made it difficult for MMA to infiltrate the surface of the protective layer at lower paving temperatures, which was about 165°C and 240°C for EA and GA, respectively. The Tg of MMA was about 85.15°C, so at 165°C, MMA could not fully infiltrate the mixture surface before it

Table 4: Pull-off/shear test results of "poly(MMA-r-nBA)/MMA + asphalt mixture" composite structure at different temperatures.

Temperature (°C)	Composite strtucre	Average tensile strength (MPa)	Failure mode	Average shear strength (MPa)	Failure mode
25	poly(MMA-r-nBA)+GA	0.75	Adhesive failure	0.35	Adhesive failure
	poly(MMA-r-nBA)+EA	0.16	Adhesive failure	0.38	Adhesive failure
	MMA + GA	0.9	Adhesive failure	0.7	Adhesive failure
	MMA + EA	0.02	Adhesive failure	0.03	Adhesive failure
60	poly(MMA-r-nBA)+GA	0.14	Adhesive failure	0.13	Asphalt mixture cracking
	poly(MMA-r-nBA)+EA	0.06	Adhesive failure	0.09	Adhesive failure
	MMA + GA	0.15	Adhesive failure	0.14	Adhesive failure
	MMA + EA	0.00	Adhesive failure	0.00	Adhesive failure

lost its fluidity. At this time, MMA would not penetrate the pores of the asphalt mixture surface to form a mechanical interaction and could not form a good intermolecular force with the asphalt binder. However, the Tg of poly(MMA-r-nBA) was 30.01°C. The lower Tg allowed the poly(MMA-r-nBA) material to maintain a viscous flow state at the EA paving temperatures.

The better flexibility and lower Tg of the poly(MMA-r-nBA) contributed to the compatibility between poly(MMA-r-nBA) and EA. From the experimental results in Table 4, it was clear that the adhesive/shear strength between the interface with the asphalt mixture provided by MMA was almost the same as that of poly(MMA-r-nBA). The bond damage between the asphalt mixture and steel plate occurred mainly at the "WAL-asphalt mixture" interface. Moreover, the material price of MMA (5.98 $/kg) was 1.4 times that of poly(MMA-r-nBA) (4.19 $/kg). Therefore, poly(MMA-r-nBA) provided comparable interfacial adhesive strength to MMA materials at a reduced cost. The poly(MMA-r-nBA) as a new steel bridge deck WAL adhesive has a good economy, excellent toughness, and compatibility on various substrates.

4. Conclusions

This article performed microscopic characterization, pull-off, and direct shear experiments on the poly(MMA-r-nBA) waterproofing material after computer simulation to determine the optimal molecular ratio. The polymer toughening mechanism was explored, and the performance of MMA and poly(MMA-r-nBA) were compared and analyzed. The main conclusions were as follows:

The introduction of nBA reduced the glass transition temperature and the minimum film formation temperature of the poly(MMA-r-nBA) copolymer and improved the high-temperature stability and flexibility.

The results of ATR-FTIR microscopic tests confirmed that nBA was indeed attached in the MMA structure, which was consistent with the theoretical reaction structure. SEM testing explores the fractured nature of poly(MMA-r-nBA) polymers from a high depth-of-field perspective. The results proved that the increase in nBA monomer reduced the material stiffness and increased the tensile fracture rate.

Adhesive and shear performance of both poly(MMA-r-nBA) and MMA would reduce with the elevated temperature. However, poly(MMA-r-nBA) provided comparable interfacial adhesive strength to MMA materials at a reduced cost. Also, poly(MMA-r-nBA) has excellent toughness and compatibility over various substrates as WAL adhesives for the steel bridge deck.

Data Availability

The data used to support the findings of this study are available from the corresponding author upon request.

Conflicts of Interest

The author declares that she has no known competing financial interests or personal relationships that could have appeared to influence the work reported in this study.

Authors' Contributions

Mengya Zhang conceptualized the study, performed formal analysis, wrote the original draft, and reviewed and edited the article.

References

[1] J. Li, A. D. Celiz, J. Yang et al., "Tough adhesives for diverse wet surfaces," *Science*, vol. 357, no. 6349, pp. 378–381, 2017.

[2] J. Liu, C. S. Y. Tan, Z. Yu, C. Abell, and O. A. Scherman, "Tough supramolecular polymer networks with extreme stretchability and fast room-temperature self-healing," *Advanced Materials*, vol. 29, no. 22, Article ID 1605325, 2017.

[3] L. Li, Y. Bai, L. Li, S. Wang, and T. Zhang, "A superhydrophobic smart coating for flexible and wearable sensing electronics," *Advanced Materials*, vol. 29, no. 43, Article ID 1702517, 2017.

[4] Y. Lu, S. Sathasivam, J. Song, C. R. Crick, C. J. Carmalt, and I. P. Parkin, "Robust self-cleaning surfaces that function when exposed to either air or oil," *Science*, vol. 347, no. 6226, pp. 1132–1135, 2015.

[5] T. Verho, C. Bower, P. Andrew, S. Franssila, O. Ikkala, and R. H. A. Ras, "Mechanically durable superhydrophobic surfaces," *Advanced Materials*, vol. 23, no. 5, pp. 673–678, 2011.

[6] Y. Yang, M. A. G. Silva, H. Biscaia, and C. Chastre, "CFRP-to-steel bonded joints subjected to cyclic loading: an experimental study," *Composites Part B: Engineering*, vol. 146, pp. 28–41, 2018.

[7] Y. Yang, J. Zhao, S. Zhang, Z. Yang, and H. Biscaia, "Influence of salt fog and ambient condition exposure on cfrp-to-steel bonded joints," *Composites Part B: Engineering*, vol. 280, Article ID 114874, 2021.

[8] S. A. Bello, J. O. Agunsoye, S. B. Hassan, and M. G. Z. Kana, "Epoxy resin based composites, mechanical and tribological properties: a review," *Tribology in Industry*, vol. 37, no. 4, pp. 500–524, 2015.

[9] Q. J. Zhong and D. Y. Hu, "Experimental study on temperature stability of waterproof bonding material for steel bridge deck pavement (Chinese)," *China Building Waterproofing*, vol. 14, pp. 5–9, 2016.

[10] S. Özlem and J. Hacaloglu, "Thermal degradation of poly(n-butyl methacrylate), poly(n-butyl acrylate) and poly(t-butyl acrylate)," *Journal of Analytical and Applied Pyrolysis*, vol. 104, pp. 161–169, 2013.

[11] M. Zhang, P. Hao, G. Men, N. Liu, and G. Yuan, "Research on the compatibility of waterproof layer materials and asphalt mixture for steel bridge deck," *Construction and Building Materials*, vol. 269, Article ID 121346, 2021.

[12] B. Benyahia, M. A. Latifi, C. Fonteix, F. Pla, and S. Nacef, "Emulsion copolymerization of styrene and butyl acrylate in the presence of a chain transfer agent," *Chemical Engineering Science*, vol. 65, no. 2, pp. 850–869, 2010.

[13] M. Sadeghalvaad and S. Sabbaghi, "Application of TiO2/Polyacrylamide core-shell nanocomposite as an additive for controlling rheological and filtration properties of water-based drilling fluid," *Journal of Nanofluids*, vol. 6, no. 2, pp. 205–212, 2017.

[14] J.-C. Lai, J.-F. Mei, X.-Y. Jia, C.-H. Li, X.-Z. You, and Z. Bao, "A stiff and healable polymer based on dynamic-covalent boroxine bonds," *Advanced Materials*, vol. 28, no. 37, pp. 8277–8282, 2016.

[15] M. Kathan, P. Kovaříček, C. Jurissek et al., "Control of imine exchange kinetics with photoswitches to modulate self-healing in polysiloxane networks by light illumination," *Angewandte Chemie International Edition*, vol. 24, pp. 13882–13886, 2016.

[16] C.-H. Li, C. Wang, C. Keplinger et al., "A highly stretchable autonomous self-healing elastomer," *Nature Chemistry*, vol. 8, no. 6, pp. 618–624, 2016.

[17] Q. Zhang, S. Niu, L. Wang et al., "An elastic autonomous self-healing capacitive sensor based on a dynamic dual crosslinked chemical system," *Advanced Materials*, vol. 30, no. 33, Article ID 1801435, 2018.

[18] Q. Huang, Z. Qian, L. Chen et al., "Evaluation of epoxy asphalt rubber with silane coupling agent used as tack coat for seasonally frozen orthotropic steel bridge decks," *Construction and Building Materials*, vol. 241, Article ID 117957, 2020.

[19] M. Shioya, Y. Kuroyanagi, M. Ryu, and J. Morikawa, "Analysis of the adhesive properties of carbon nanotube- and graphene oxide nanoribbon-dispersed aliphatic epoxy resins based on the Maxwell model," *International Journal of Adhesion and Adhesives*, vol. 84, pp. 27–36, 2018.

[20] I. Zaborniak, P. Chmielarz, M. R. Martinez, and K. Z. K. Wolski, "Synthesis of high molecular weight poly(n-butyl acrylate) macromolecules via seATRP: from polymer stars to molecular bottlebrushes," *European Polymer Journal*, vol. 126, Article ID 109566, 2020.

[21] W. Miao, W. Cheng, Z. Wang, R. Wang, J. Peng, and Q. Zhu, "Influence of n-butyl acrylate and maleic anhydride copolymer on the structure and properties of phenolic resin," *Materials Today Communications*, vol. 23, Article ID 100879, 2020.

[22] M. W. Urban, D. Davydovich, Y. Yang, and T. Y. L. Demir, "Key-and-lock commodity self-healing copolymers," *Science*, vol. 362, no. 6411, pp. 220–225, 2018.

[23] Y. I. Odarchenko, M. Rosenthal, A. J. Kimenai et al., "Structure formation and hydrogen bonding in all-aliphatic segmented copolymers with uniform hard segments," *Acta Biomaterialia*, vol. 9, no. 4, pp. 6143–6149, 2013.

[24] M. Bounekhel and I. C. Mcneill, "Preparation and thermal degradation studies of telechelic poly(methyl methacrylate)," *Polymer Degradation and Stability*, vol. 65, no. 3, pp. 443–448, 1999.

[25] J. Sun, J. Su, C. Ma et al., "Fabrication and mechanical properties of engineered protein-based adhesives and fibers," *Advanced Materials*, vol. 32, no. 6, Article ID 1906360, 2020.

[26] Z. Zeng, F. Jiang, Y. Yue et al., "Flexible and ultrathin waterproof cellular membranes based on high-conjunction metal-wrapped polymer nanofibers for electromagnetic interference shielding," *Advanced Materials*, vol. 32, no. 19, Article ID 1908496, 2020.

[27] M. Kikuchil, "Dimple fracture simulation of fracture specimen under different constraint conditions," *Cmes-Comp Model. Eng.*vol. 11, no. 2, pp. 49–59, 2006.

[28] M. Zhang, P. Hao, and Y. Li, "Interfacial adhesive property in "asphalt mixture-PMA copolymer-steel plate" system: experimental and molecular dynamics simulation," *Construction and Building Materials*, vol. 281, Article ID 122529, 2021.